Collisional excitation of N+(3 P) in interstellar clouds

Marie Gueguen, François Lique

MNRAS 000, 1–7 (2022) Preprint 9 May 2023 Compiled using MNRAS LATEX style file v3.0

Collisional excitation of $N^+(^3P)$ in interstellar clouds

Marie Gueguen,* François Lique†
Univ Rennes, CNRS, IPR (Institut de Physique de Rennes) - UMR 6251, F-35000 Rennes, France.

Accepted XXX. Received YYY; in original form ZZZ

ABSTRACT

The detection of the N^+ ion in ionized interstellar regions, as well as its use as a tracer for atomic nitrogen (N) in interstellar media, make it an interesting ion from the astrophysical point of view. Accurate determination of the N^+ abundance in the interstellar clouds requires detailed modeling of its excitation conditions. Hence, collisional excitation induced by the dominant interstellar species has to be studied. In this paper, we study the collisional excitation of N^+ by He and H_2. We provide new potential energy surfaces describing the interactions between N^+ and He and between N^+ and H_2 considered as a structureless collider. Quantum calculations of the excitation cross sections for collisions of N^+ with He and H_2 are provided, as well as the first excitation rate coefficients for N^+ induced by these two species. The results are compared to collisional data for the excitation induced by electrons. It is shown that the excitation of N^+ by a neutral collider can play a significant role in weakly ionized regions as well as in warm molecular clouds.

Key words: astrochemistry molecular data ISM:abundances

1 INTRODUCTION

N and N_2, the dominant nitrogen-bearing elements (Le Gal et al. 2014; Maret et al. 2006) in the interstellar medium (ISM), are respectively impossible and difficult to detect spectroscopically through infrared or millimeter-wavelength transitions. This is due to the fact that N and N_2 do not have fine structure levels and dipole moment, respectively. Proxy are thus used to infer their abundance in interstellar clouds (Le Gal et al. 2014). The N^+ ion is detected in the warm and ionized interstellar medium (Langer et al. 2017; Doherty et al. 2020; Goldsmith et al. 2015) and could qualify as such a proxy. Indeed, N^+ is considered as an important tracer for N in (fully) ionized regions. It can also be used for discriminating between fully and weakly ionized regions. Despite not (yet) detected in cold molecular clouds, N+ is also expected to be important constituant of such region that initiates the nitrogen chemistry and particularly the formation of ubiquitous ammonia (Dislaire et al. 2012).

The spin-orbit interaction in ionized nitrogen N^+ splits its ground electronic state into a triplet of fine-structure levels ^3P_j with $j = 0, 1, 2$. The $^3P_1$ and $^3P_2$ levels are at 48.738 cm^{-1} and 130.8 cm^{-1} above $^3P_0$ (Shen et al. 2022), respectively. Transitions with $\Delta j = 1$ are allowed and thus make the detection of N^+ possible.

Collisional data are needed for interpreting N^+ observations and estimating physical conditions. Indeed, in environments that do not reach local thermodynamic equilibrium (LTE), the population of N^+ levels has to be modeled through the competition between radiative and collisional processes (Roueff & Lique 2013). Collisional data for N^+, although known for the excitation induced by electrons (Tayal 2011), are still missing for the excitation induced by heavier species such as He or H_2. Without them, astrophysical observations must be interpreted on the basis of the LTE assumption, which does not allow to make the most of the highly resolved molecular spectra that recently developed facilities do offer. Due to the lack of collisional data available for N^+ with the main neutral colliders (He, H and H_2[1]), Persson et al. (2014) had to model spectral observations based on scaled C-H rate coefficients. Such approximation may lead to significant errors in the observations interpretation and exploitation.

Calculation of these data requires first to compute an interaction potential between N^+ and the projectile (H_2 or He in the present study). He and H2 are the dominant colliders in cold molecular clouds where N+ is expected to play a significant role in nitrogen chemistry. In warm (ionized) clouds where N+ has been detected, H is the dominant neutral projectile. Calculations with H projectile are difficult to perform and we estimate that calculations with He and H2 projectiles can serve as template for the modelling the impact of neutral colliders (Roueff & Lique 2013). Two studies (Aïssaoui et al. 2020; Soldán & Hutson 2002) have provided potential energy curves (henceforth PECs) for N^+–He in the last two decades. However, their PECs are based on coupled-cluster methods with an incomplete basis. Nowadays, computing facilities should allow to improve the description of the N^+–He interaction. At the opposite, the determination of global N^+–H_2 potential energy surfaces (henceforth PESs) involved in the collisional process as well as the non adiabatic and spin orbit couplings between them is a very challenging task because of the reactive nature of the system. In order to overcome this difficulty, Gómez-Carrasco et al. (2022) have recently provided PESs for the reactant and product channels separately without considering the intermediate region and have simulated the dynamics of the $N^+ + H_2 \rightarrow NH^+ + H$ reaction using statistical theories.

* E-mail: marie.gueguen@univ-rennes.fr
† E-mail: francois.lique@univ-rennes.fr

[1] H_2 is usually by far the dominant collider in molecular clouds.

Full dimension quantum time-independent close-coupling calculations is the method of choice to obtain accurate collisional rate coefficients. Such an approach can be easily used for non-reactive collisional systems such as N^+–He. However, in the case of reactive systems such as N^+–H_2 (Gómez-Carrasco et al. 2022), this approach is impractical due to its memory and CPU requirements and approximate treatments have to be considered.

In this paper, we provide new highly accurate PECs for studying the collisional excitation of N^+ by He. We also provide PECs averaged over H_2 rotations for N^+–H_2 interaction. This later potential relies on important approximations, as it treats this system as a non-reactive system. Then, we report inelastic cross sections of the collisional systems from quantum close-coupling (CC) calculations, and we derive collisional data for both systems. This paper is organized as follows: in section 2, we present the new N^+–He PECs, as well as the spherically averaged PECs for the N^+–H_2 interaction. Section 3 presents the inelastic cross sections and the rate coefficients obtained from our new PECs. Finally, in section 4, we discuss our results and their astrophysical implications.

2 N^+–HE AND N^+–H_2 INTERACTION POTENTIALS

2.1 N^+–He potential energy curves

The interaction of a closed-shell rare-gas atom with a ^3P-state atom gives rise to two electronic states: a $^3\Sigma$ state and a doubly degenerate $^3\Pi$ state. *Ab initio* calculations were performed for internuclear distances in the range $1.8 < R < 100\ a_0$ for the $^3\Sigma$ electronic state and $2.5 < R < 100\ a_0$ for the $^3\Pi$ electronic state, using the spin restricted coupled cluster method with single and double excitation and a perturbative treatment of triple excitation [RCCSD(T)] (Knowles et al. 1993, 2000) and the MOLPRO package (Werner et al. 2020).

As is usually the case in standard *ab initio* calculations, the spin-orbit coupling was neglected, but taken into account in the scattering calculations. Calculations were performed with the augmented correlation consistent [aug-cc-pVXZ (X=T, Q, 5)] basis set and extrapolated to the complete basis set (CBS) using the procedure of Peterson et al. (1994). Standard corrections were applied to account for the basis set superposition error (BSSE), using Boys & Bernardi (1970)'s procedure.

In order to obtain an analytical representation, suitable for scattering calculations, we have used the following procedure. For short-range (SR) R-distances, we have used the Born-Mayer formula that traditionally describes the ion-atom curves such as:

$$V_{(SR)}(R) = \alpha \exp(-\beta R) \tag{1}$$

with α and β being constants parameters (Pauly 1979). Three coefficients (C_4, C_6, C_8) adjusted from the *ab initio* energy values at 15, 20 and 25 a_0 were used to describe the PES at long-range (LR) R-distances using the following analytic formula:

$$V_{LR}(R) = \frac{C_4}{R^4} + \frac{C_6}{R^6} + \frac{C_8}{R^8} \tag{2}$$

Table 1 shows the value calculated for the short-range and long-range parameters.

C_4, C_6 and C_8 correspond to the leading terms in the long range expansion of the N^+–He interaction: dipole-dipole induction coefficient, dispersion and induction coefficients, respectively (Côté & Dalgarno 2000; Bouchelaghem & Bouledroua 2014).

Parameters	$^3\Sigma$	$^3\Pi$
α	95.65	19.38
β	4.09	2.12
C_4	0.69	-0.69
C_6	7.54	-3.50
C_8	78.67	-6.69

Table 1. The values adopted for the short-range and long-range parameters. All units are in a.u.

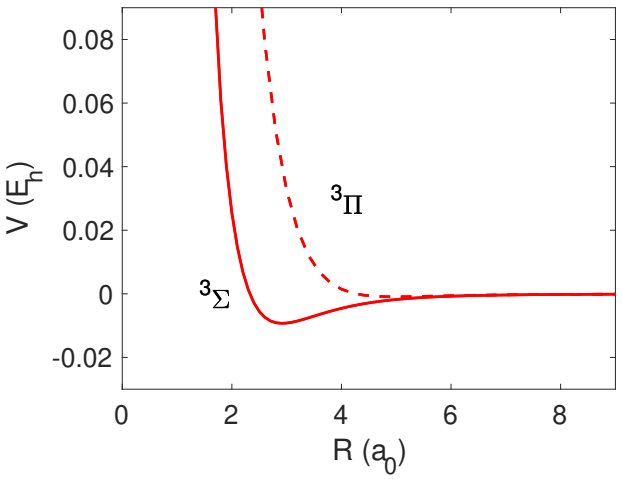

Figure 1. Potential energy curves for the HeN^+ complex.

Table 2. Characterization of the HeN^+ PECs obtained by SH02, A20 and in this work.

	$^3\Sigma$		$^3\Pi$	
	R (a_0)	V (cm^{-1})	R (a_0)	V (cm^{-1})
SH02	2.9	-2004.85	5.0	-202.49
A20	3.0	-2041.03	5.0	-213.15
This work	2.9	-2037.33	5.0	-204.05

Finally, we used a cubic spline for interpolating smoothly our *ab initio* data points.

Figure 1 presents the N^+–He PECs obtained. The PECs are characterized by a minimum at 2.9 a_0 of -2037 cm^{-1} for the $^3\Sigma$ state and at 5.0 a_0 of -204.05 cm^{-1} for the $^3\Pi$ state. The well is thus much deeper for $^3\Sigma$ than for $^3\Pi$, which can easily be explained since the $^3\Sigma$ state corresponds to approaches of He along the unoccupied p orbital. In that case, He can get much closer to the ion and the well will thus be much deeper. Note that our results, although improving upon former PECs published by Soldán & Hutson (2002) and Aïssaoui et al. (2020) as relying on an extrapolation to the complete basis set, are in good agreement with them, with a difference of less than 0.2 % and 4.5% for the $^3\Sigma$ and $^3\Pi$ minima, respectively. Table 2 shows and compares the main characteristics of the PECs obtained by Soldán & Hutson (2002) (SH02), Aïssaoui et al. (2020) (A20) and this work.

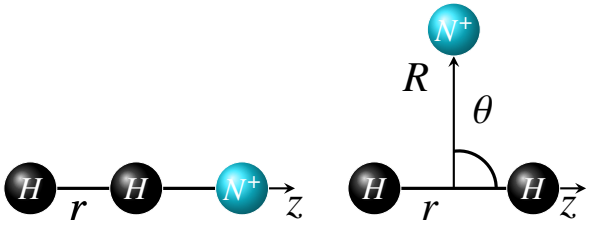

Figure 2. N$^+$–H$_2$ collisional system in Jacobi coordinates. On the left, the linear approach corresponding to $\theta = 0$ degree. On the right, the perpendicular approach, where $\theta = 90$ degree.

2.2 N$^+$–H$_2$ spherically averaged potential energy curves

As mentioned in the introduction, obtaining global PESs for the H_2N^+ system is highly challenging because of the reactive nature of this system, as exemplified by the work done by Gómez-Carrasco et al. (2022). Indeed, these authors only computed a PES for the entrance ($N^+ + H_2$) and exit ($NH^+ + H$) channel, neglecting the intermediate (NH_2^+) region. Here, we used a different strategy and we selected a reduced dimensional approach, where the H_2 molecule is described as a structureless sphere. This approach requires to keep the intermolecular distance between the two H atoms fixed, which amounts to treating the complex as non-reactive. Then, we averaged the PECs thus obtained for limited H_2 orientations which means that we treat H_2 as a pseudo-atom rather than as a molecule.

Hence, as shown in Figure 2, the N$^+$–H$_2$ PECs are described by the two Jacobi coordinates R, the distance from the center of mass of H_2 molecules to the N^+ atom, and θ, the angle between R and the H_2 bond axis r. We considered that the H_2 molecule only approaches the ion linearly ($\theta = 0$ degree) or perpendicularly ($\theta = 90$ degree).

Ab initio calculations were performed using the RCCSD(T) approach with the augmented correlation consistent triple zeta (aug-cc-pVTZ) basis set. We chose to stay at this level of precision given the level of approximations involved in the spherically-averaged approach that we adopted. Calculations were performed in the range $1.3 < R < 100\ a_0$ for all electronic states considered here. Interactions between the ion N^+ and H_2 along the linear approach give rise to three electronic states: a $^3\Sigma$ state and two degenerate $^3\Pi$ states. Regarding the perpendicular approach, the degeneracy disappears and the $^3\Sigma$ and $^3\Pi$ state split into $^3A_2$ (for $^3\Sigma$), $^3B_1$ and $^3B_2$ (for $^3\Pi$) electronic states in the C_{2v} symmetry group respectively.

Thus, we calculated a total of five PECs, two for the linear approach ($^3\Sigma$ and $^3\Pi$) and three for the perpendicular approach ($^3A_2$, $^3B_1$ and $^3B_2$). Figure 3 presents the five PECs obtained.

N$^+$–H$_2$ spherically averaged PECs ($V^i_{av}(R)$) are obtained by averaging over the linear and perpendicular approaches using the following formula, with V^i the interaction potential at a given distance R:

$$V^i_{av}(R) = \frac{1}{5}[2V^i(R, \theta = 0°) + 3V^i(R, \theta = 90°)] \quad (3)$$

Note that we tested three different ways of proceeding to this average to get the N$^+$–H$_2$ PECs for $^3\Sigma$ and $^3\Pi$ pseudo states. First, the average was done over the linear potential and the perpendicular potential using only the $^3B_1$ state and the $^3A_2$ state for the latter; only the $^3B_2$ state and the $^3A_2$ state; and finally an average over the $^3B_1$ and the $^3B_2$ state and the $^3A_2$ state. Given that we did not observe significant differences between the final PECs thus obtained, we adopted the averaged curve over $^3B_1$ and $^3B_2$ for the scattering calculations, as displayed in Figure 4, albeit physically meaningless. Such a weak influence of the use of $^3B_1$ or $^3B_2$ states for the generation of the N$^+$–H$_2$ spherically averaged PECs can be explained by the fact that the two $^3B_1$ or $^3B_2$ states are almost degenerate up to R-distances of 2.4 a_0.

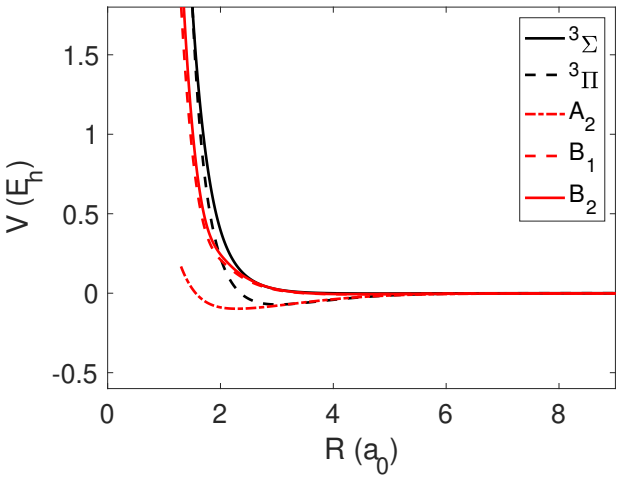

Figure 3. Potential energy curves for the five orientations of N$^+$–H$_2$. Black lines correspond to the linear approaches, and the red lines to the perpendicular ones.

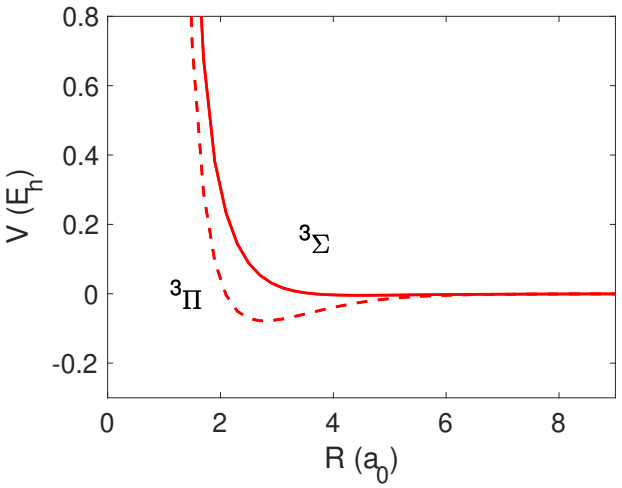

Figure 4. Potential energy curves for N$^+$–H$_2$.

Similarly to what has been done for the analytical representation of the N$^+$–He PECs, the extrapolation to short-range distances is based on the Born-Mayer formula, with $\alpha = 1223.76$ and $\beta = 3.05$ a.u. for the $^3\Sigma$ state and $\alpha = 9328.61$ and $\beta = 8.42$ a.u. for $^3\Pi$ state. The extrapolation for long-range distances relies on multipolar expansion (R^{-n} terms) through the C_3, C_4 and C_5 coefficients, whose value is determined from long range *ab initio* points and correspond respectively to 0.0514, -2.7823 and 1.0847 a.u. for the Σ state; and 0.0619, -3.2309 and 3.2563 a.u. for the Π state. Finally, *ab initio* points were smoothly connected on the basis of a cubic spline interpolation.

Figure 4 presents the PECs obtained for the $^3\Sigma$ and the $^3\Pi$ states through this spherically averaged approach. Compared to the PECs of N$^+$–He, we observe an inversion of the states's hierarchy: the potential

Table 3. Characterization of the N^+–H_2 PECs according to this work.

	$^3\Sigma$		$^3\Pi$	
	R (a_0)	V (cm^{-1})	R (a_0)	V (cm^{-1})
This work	4.5	-968.32	2.7	-17121.22

well is deeper for the $^3\Pi$ state than for $^3\Sigma$ one, and the minima are much deeper than for He (see Table 3 for PECs characteristics).

3 QUANTUM SCATTERING CALCULATIONS

3.1 State-to-state cross sections

Scattering calculations for N^+–He and N^+–H_2 were performed with the close-coupling approach (Arthurs & Dalgarno 1960), following the method described by Alexander et al. (1983); Orlikowski & Alexander (1984) for ^3P-atom - structureless projectile collisions and implemented in the HIBRIDON code (Alexander et al. 2021). The spin-orbit couplings dependence on R was neglected. As is usually done, we use the asymptotic experimental spin-orbit splittings of N^+ (^3P), $\Delta_{j=1}$= 48.738 cm^{-1} and $\Delta_{j=2}$= 130.8 cm^{-1} respectively, to determine spin-orbit corrected potential energy curves (PECs). The hybrid log-derivative/airy propagator implemented in the HIBRIDON code has been used, starting from R_{min} = 1.5 a_0 to R_{mid} = 25 a_0 for the log-derivative method, and from R_{mid} = 25 a_0 to R_{max} = 250 a_0 for the Airy propagator for N^+–He collisions and from R_{min} = 1.2 a_0 to R_{mid} = 40 a_0 for the log-derivative method, and from R_{mid} = 40 a_0 to R_{max} = 200 a_0 for the Airy propagator for N^+–H_2 collisions. All these parameters were adequate to ensure a convergence of cross sections to better than 1%. These calculations have been performed for total energies up to 10000 cm^{-1}. For the energy grid, we have used a variable step. For energies smaller than 100 cm^{-1}, the step is 0.2 cm^{-1}. Then, between 100 and 200 cm^{-1}, the step is increased to 0.5 cm^{-1}, between 200 and 400 cm^{-1} to 2, between 400 and 600 cm^{-1} to 10. Finally, between 600 and 1000 cm^{-1}, the step is increased to 20 cm^{-1} and to 100 cm^{-1} above that limit. The reduced mass of the complexes were μ = 3.11 u for N^+–He and μ = 1.76 u for N^+–H_2. For the former, the maximum total angular momentum considered was J = 20 for energies lower than 300 cm^{-1}, J = 30 for energies between 300 and 1000, J = 50 for energies between 1000 and 2500, and J = 80 for energies greater than 2500 cm^{-1}. For the latter, the maximum total angular momentum considered was J = 30 for energies lower than 300 cm^{-1}, J = 50 for energies between 300 and 1000 and J = 80 for energies superior to 1000 cm^{-1}.

Figure 5 shows the state-to-state cross-sections for the de-excitation transitions of N^+ induced by collisions with He. We can see that the transition from $^3P_2$ to $^3P_1$ dominates the de-excitation process and that the $^3P_1$ to $^3P_0$ transition is weak, which is not surprising as this transition is classically forbidden (Monteiro & Flower 1987). This behavior has been noticed for others atoms with a ^3P electronic ground state in collision with He (Alexander et al. 1983; Monteiro & Flower 1987; Lique et al. 2018).

Figure 6 presents the state-to-state cross-sections of N^+ with H_2. Cross-sections at low collision energy (E_c) exhibit strong Feshbach and shape resonances due to the attractive potential wells (Costes & Naulin 2016). These resonances disappear when E_c is large compared to the well depth. The transition from $^3P_2$ to $^3P_1$ is the most efficient; and the transition from $^3P_1$ to $^3P_0$ dominates over the $^3P_2$ to $^3P_0$ at low energy, thanks to a coupling through $^3P_2$ that is stronger at low energy, as noted in Alexander et al. (1983).

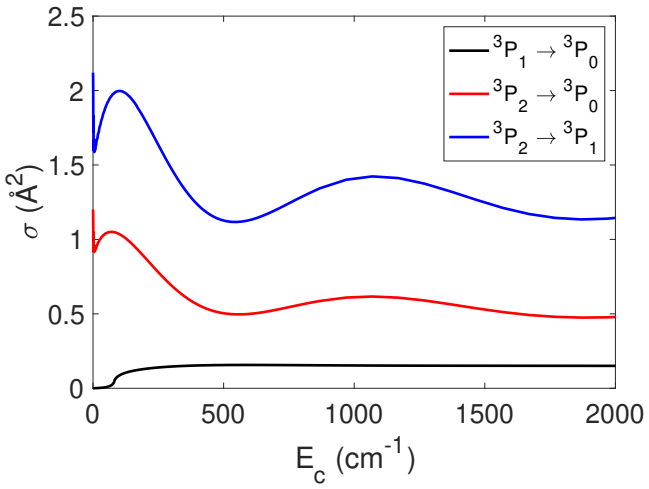

Figure 5. State-to-state cross-sections of N^+ with He as a function of energy.

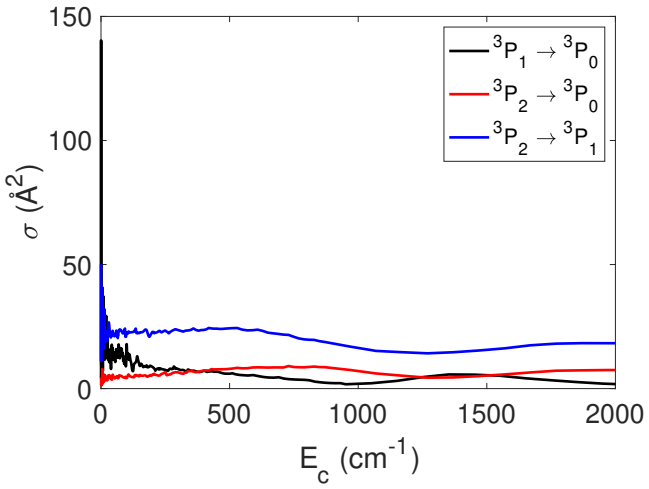

Figure 6. State-to-state cross-sections of N^+ with H_2 as a function of energy.

3.2 Rate coefficients

From the inelastic cross sections $\sigma(E_c)$, one can derive the corresponding rate coefficients at temperature T by an averaging over the collision energy (E_c):

$$k_{i\rightarrow j}(T) = \left(\frac{8}{\pi\mu k_B^3 T^3}\right)^{\frac{1}{2}} \int_0^{+\infty} \sigma_{i\rightarrow j} E_c \exp\left(\frac{-E_c}{k_B T}\right) dE_c \quad (4)$$

where k_B is the Boltzmann constant, and i and j denote the initial and final levels of the target, respectively. Calculations of the cross sections at total energies up to 10000 cm^{-1} allow the determination of rates up to 2000 K without loss of accuracy.

Unsurprisingly, the rate coefficients derived from the N^+–He cross-sections reflects the hierarchy of transitions observed for the latter, as shown in Figure 7. The transition from the $^3P_2$ state to the $^3P_1$

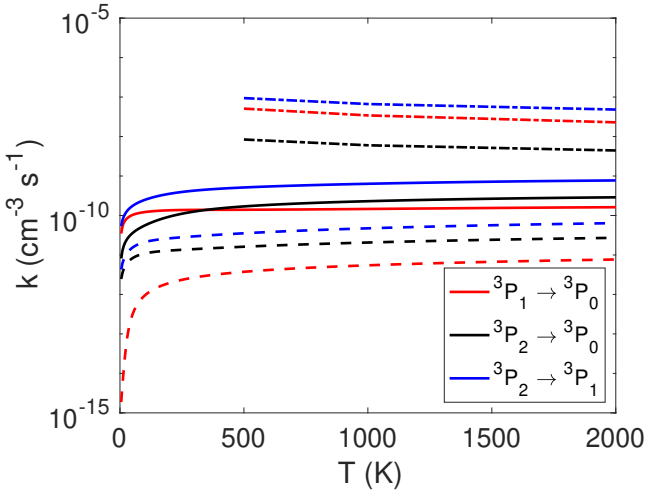

Figure 7. Comparison between collisional rate coefficients for N$^+$-He (dashed lines), for N$^+$-H$_2$ (solid lines) and for N$^+$-e (dashed dotted lines) (Tayal 2011) as a function of temperature.

one largely dominates the other transitions and the $^3P_1$ to $^3P_0$ remains negligible. Likewise, in the case of N$^+$–H$_2$, the same behavior is observed for the transitions's hierarchy with respect to rate coefficients than for the cross-sections, with the transition from $3P_1$ to $3P_0$ dominating over the $3P_2$ to $3P_0$ up to ~500 K.

3.3 Discussion and comparison with electronic excitation rate coefficients

As mentioned in the introduction, H$_2$ is the most abundant partner in interstellar molecular clouds and thus the dominant collisional partner in such media. Despite significant update for many interstellar atoms and molecules (Roueff & Lique 2013; van der Tak et al. 2020), collisional data are still difficult to produce for collisions with H$_2$, especially for reactive molecules and ions. When data for collisions with He are available, it has often been proposed to derive H$_2$-rate coefficients from He-rate coefficients calculated for the same molecule. Such an approach (Lique et al. 2008; Schöier et al. 2005) consists in assuming that the excitation cross-sections are similar for both colliding systems and that the rate coefficients would only differ by a scaling factor, that corresponds to the square root of the ratio between the reduced masses appearing in the conversion of the cross sections into rate coefficients [Eq. 4]. Hence, the following scaling relationship could be used in our case:

$$k^{\rm He} \simeq 1.4 \times k^{\rm H_2}. \quad (5)$$

Note that this approximation is only supposed to be used for H$_2$ at low temperatures (e.g., when most H$_2$ is in its ground state), but has already been challenged for many species; for a general criticism of this assumption see Roueff & Lique (2013).

Here, we discuss the validity of estimating H$_2$-rate coefficients from He ones when it comes to our system, i.e, to determine whether He can be a good template model for understanding and quantifying the collisional excitation of N$^+$ by H$_2$. One caveat that must be addressed in order to answer this question is the following: we do not have state-of-the-art results for H$_2$, but only quantum scattering calculations performed on the basis of interaction potentials containing important approximations. N$^+$–H$_2$ was treated as a non-reactive system given that the intermolecular distance between the two H was fixed, and H$_2$ was treated as a pseudo-atom given that we averaged the PESs over H$_2$ rotations. There is no way to determine how these approximations impact the collisional rate coefficients obtained for N$^+$–H$_2$. We have reasons however to believe that, albeit these approximations, our calculations may provide the right order of magnitude of the fine structure resolved rate coefficients. Thus, we may be allowed to use them at least to interpret the exact results obtained for He and to determine on this basis whether the 1.4 scaling factor assumption is valid for this system.

We see in Figs. 5 and 6 that, as expected, given the deeper potential well in the N$^+$–H$_2$ interaction as compared to N$^+$–He one, H$_2$-cross-sections are much larger for the He ones. A difference of one order of magnitude can be observed between the corresponding cross-sections. The order of magnitude of the cross sections is not the only difference between the two collisional complexes. The behavior of the state-to-state cross sections observed for the N$^+$–H$_2$ system is very different from the one observed for N$^+$–He one. Whereas the $3P_1$ to $3P_0$ transition induced by He collisions was negligible, for N$^+$–H$_2$ collisions, it is not only much more important proportionally, and it actually dominates over the the $^3P_2$ to $^3P_0$ transition thanks to an efficient coupling of the $^3P_0$ and $^3P_1$ states with the $^3P_2$ one. Our results show that He is not a correct model to describe the excitation of N$^+$ induced by H$_2$.

In astrophysical media where N$^+$ is found, electronic collisions are also supposed to play a significant role for the excitation of N$^+$. Thus, it is important to compare the efficiency of electron and neutral collisional partners (He and H$_2$) for the excitation of N$^+$. In Fig. 7, we compare rate coefficients for the de-excitation of N$^+$ induced by electron impact (Tayal 2011) to the de-excitation rate coefficients induced by He and H$_2$ collisions computed in this work. Rate coefficients for the (de-)excitation of N$^+$ by electrons are ~ 2-3 orders of magnitude higher than that of the collisional (de-)excitation induced by H$_2$. Such a difference suggests that in astrophysical environments where the electronic fraction is low ($n_{e-} \leq 10^{-4}$), collisions with H$_2$ will compete or even dominate the excitation of N$^+$, and indicates that N$^+$–H$_2$ collisional data should be used in order to accurately model N$^+$ excitation in interstellar clouds. At the opposite, in highly ionized media, the electronic excitation will dominate.

4 THE EXCITATION OF N$^+$ IN INTERSTELLAR MEDIA

Calculations of critical densities can help to identify more precisely when such N$^+$ rate coefficients would need to be considered in radiative transfer models. The concept of critical density refers to the ratio between the Einstein coefficients, expressed in s^{-1} and the collisional de-excitation rate coefficients for a given transition (in cm^{-3} s^{-1}). Put differently, the ratio of the Einstein coefficients $A_{i\rightarrow j}$ to the collisional de-excitation rate coefficients $k_{i\rightarrow j}$ defines the critical density n^* of a given line, i.e, the density at which photon de-excitation and collisional de-excitation are equal.

$$n^*(T) = \frac{A_{i\rightarrow j}}{k_{i\rightarrow j}} \quad (6)$$

Above such density, LTE conditions can generally be safely assumed. Critical densities for electrons had already been calculated by Goldsmith et al. (2015), on the basis of Tayal's collisional rates. Figure 8 displays the critical densities for He, H$_2$ and electrons for the two allowed radiative transitions as a function of temperature.

It can be seen that for ionized warm media where N$^+$ has been

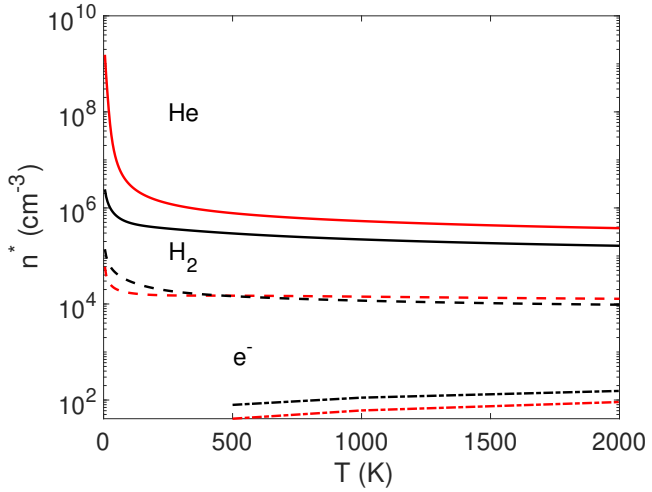

Figure 8. Critical densities for He, H_2 and electrons as a function of temperature. Red lines correspond to the $^3P_1$ to $^3P_0$ transition and black lines to the $^3P_2$ to $^3P_1$ transition.

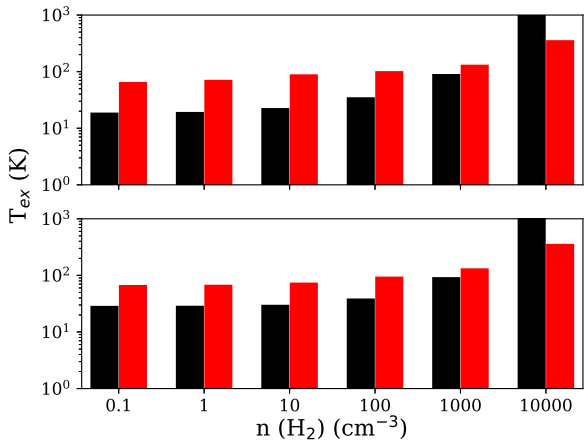

Figure 9. Excitation temperature of the $^3P_1$ to $^3P_0$ (black) and $^3P_2$ to $^3P_1$ (red) transitions as a function of the density of neutral species at 2000 K. The electronic density is kept fixed at $n_{e^-} = 10^{-1}$ cm^{-3} (upper panel) and $n_{e^-} = 1$ cm^{-3} (bottom panel).

detected (with densities lower than 10^2 cm^{-3}), LTE conditions are not met and that rate coefficients are required to model the N^+ emissions, although most often ignored to this day.

Then, we decided to test the impact of our rate coefficients on the excitation of N^+ in astrophysical media, by performing radiative transfer calculations for physical conditions corresponding to media where N^+ is detected. Non-LTE calculations were performed with the RADEX code (Van der Tak et al. 2007). Both collisional and radiative processes are taken into account. We focus on the calculation of the excitation temperature for N^+ transitions, with a background temperature of 2.73 K and a N^+ column density of 10^{14} cm^{-2}. H_2 is used as the only representative of neutral colliders.[2]

Figure 9 shows the excitation temperature of $^3P_1$ to $^3P_0$ and $^3P_2$ to $^3P_1$ transitions as a function of the density of neutral species, with the electronic density kept fixed at $n_{e^-} = 10^{-2}$ cm^{-3} and $n_{e^-} = 1$ cm^{-3}, respectively. A kinetic temperature of 2000 K[3] was adopted. One observes that at low densities of neutral species, even with a neutral to electron abundance ratio greater than 10^2, the excitation temperature remains weakly sensitive to the density of neutral species. It is only above a critical threshold of $n(H_2) \geq 10^3$-10^4 cm^{-3} that the excitation temperature increases and that the media starts to thermalize very fast as the density increases, with an excitation temperature equal to the kinetic temperature around $n(H_2) \geq 10^5$ cm^{-3}. Below this threshold, collisions are inefficient and do not contribute significantly to the excitation of the N^+ ion, regardless of the ratio neutral species to electrons and of the density of electrons. Note that this neutral density value is much higher than the one typically observed in warm ionized clouds, i.e., 0.1 to 100 cm^{-3}. Thus, environments where N^+ is detected do not satisfy the local thermodynamic equilibrium, and collisional rate coefficients are needed to appropriately model observations.

As a second application of our rate coefficients, we decided to verify assumptions made about N^+ in modeling the nitrogen chemistry in cold environments such as dark clouds. As emphasized in Dislaire et al. (2012), $N^+ + H_2 \rightarrow NH^+ + H$ is identified as a key reaction for the formation of nitrogen hydrides in dark clouds (Le Gal et al. 2014; Agúndez & Wakelam 2013; Hily-Blant et al. 2013). Whether the reaction $N^+ + H_2 \rightarrow NH^+$ is efficient enough to reproduce the observed amount of ammonia in dark clouds has actually been debated since the original claim made by Le Bourlot (1991), a claim later challenged by updated calculations of the rate coefficients for $N^+ + H_2 \rightarrow NH^+ + H$ (Dislaire et al. 2012), which felt below the critical value that had been inferred to explain the observed abundance of ammonia. However, due to the fact that in such cold environments, N^+ cannot be detected, assumptions have to be made about the distribution of its fine structure population. It is thus interesting to check the assumption according to which its population follows a LTE distribution in cold molecular clouds.

In such environments, the exact population of N^+ fine structure levels is not known and can influence the reactivity of N^+. LTE conditions are usually assumed but not checked because of the lack of collisional data (Gómez-Carrasco et al. 2022). Thus, we decided to perform radiative transfer calculations to determine the population levels of the fine structure levels of N^+ as a function of the density of neutral species ($n(H_2)$), where 'neutral species' refer to 90% of H_2 and 10 % of He, at 10, 20 and 50 K respectively (see Fig. 10). At 10K, as could have been anticipated, almost 100% of N^+ is in its ground state (not shown here), even at high densities according to the LTE distribution. But the level population changes as the temperature increases: at 20 K already, one observes 2 to 5% of N^+ in level $^3P_1$ at densities of 10^4–10^5 cm^{-3}. At 50 K, 20 to 30% of the whole N^+ is in the $^3P_1$ level for a density of neutral species of 10^4–10^5 cm^{-3}. Such values are below the LTE conditions that predict ~ 10 % and ~ 40% of N^+ is in $^3P_1$ level, respectively. Given that the $N^+ + H_2 \rightarrow NH^+ + H$ rate coefficients depends on the N^+ energy level population, this means that the reaction will not happen as predicted by the model. This could possibly have an important impact on the determination

[2] In such media, H is expected to be the dominant neutral collider and our results should be consider with cautious despite the fact the H_2 and H–rate coefficients are usually of similar magnitude (Schöier et al. 2005).

[3] N^+ has been detected in interstellar clouds with a typical temperature of ~ 8000 K but we restrict our models at 2000 K in agreement with the temperature range of our new data. We anticipate that because of the weak dependence of the rate coefficients, the results obtained at 2000 K will not vary significantly at 8000 K.

of the age of the clouds when the abundance of NH_3 is taken as the main tracer of it.

5 CONCLUSION

We have calculated new PECs for N^+–He at the RCCSD(T) level of theory with an extrapolation to the complete basis set. The calculations was found to be in good agreement with former theoretical studies. Using these new PECs, we have performed close-coupling calculations in order to determine collisional excitation cross sections for N^+–He and derive collisional rate coefficients.

N^+–H_2 have also been studied. These data have been computed also using RCCSD(T) approach on the basis of a spherically averaged approach to the potential energy curves for N^+–H_2, relying on important approximations. The comparison of the N^+–H_2 rate coefficients with the N^+-He one shows that significant differences exist. The differences are of such nature, e.g. differences in the hierarchy of different de-excitation transitions, that even scaled by the square root of the collision reduced mass, the He rate coefficients cannot be reasonable approximation to the N^+–H_2 rate coefficients.

Then, we considered the astrophysical consequences of our calculations. First, we have shown that media where N^+ is typically observed are not at LTE, and that LTE conditions are reached only for densities much higher than the typical conditions of warm ionized clouds. This illustrates the importance of taking into account the collisional rates coefficients. Furthermore, we have tested some important assumptions that are traditionally part of the modelling of nitrogen and ammonia. Our results show that the assumption of LTE distribution of the N^+ energy levels at temperatures below 50 K is not verified above 10 K. This could have an important impact on the modeling of ammonia, especially on the determination of the age of the clouds where N^+ is detected. Finally, we emphasize that the present study should be completed by the theoretical study of the collisional excitation of N+ by H and H+, the dominant heavy projectiles in warm (ionized) clouds in order to fully interpret and exploit the N+ observations recently performed.

ACKNOWLEDGEMENTS

This project received funding from the European Research Council (ERC) under the European Union Horizon 2020 research and innovation program (Grant Agreement No. 811363) and from the European Union Horizon 2020 research and innovation program under the Marie Slodowska-Curie grant agreement No.101026214.

DATA AVAILABILITY

The data underlying this article will be made available through the EMAA[4], LAMDA (Schöier et al. 2005; van der Tak et al. 2020) and BASECOL (Dubernet, M.-L. et al. 2013) data bases. The PECs computed in this work are available fron the authors upon request.

REFERENCES

Agúndez M., Wakelam V., 2013, Chemical Reviews, 113, 8710
Aïssaoui L., Knowles P. J., Bouledroua M., 2020, The European Physical Journal D, 74, 1
Alexander M. H., Orlikowski T., Straub J. E., 1983, Physical Review A, 28, 73
Alexander M., Manolopoulos H., Werner D. E. e. a., 2021, HIBRIDON is a package of programs for the time-independent quantum treatment of inelastic collisions and photodissociation
Arthurs A. M., Dalgarno A., 1960, Proceedings of the Royal Society of London. Series A. Mathematical and Physical Sciences, 256, 540
Bouchelaghem F., Bouledroua M., 2014, Physical Chemistry Chemical Physics, 16, 1875
Boys S., Bernardi F., 1970, Mclean AD (1973) J Chem Phys, 59, 4557
Costes M., Naulin C., 2016, Chemical Science, 7, 2462
Côté R., Dalgarno A., 2000, Physical Review A, 62, 012709
Dislaire V., Hily-Blant P., Faure A., Maret S., Bacmann A., Des Forêts G. P., 2012, Astronomy & Astrophysics, 537, A20
Doherty M., Geach J., Ivison R., Dye S., 2020, The Astrophysical Journal, 905, 152
Dubernet, M.-L. et al., 2013, A&A, 553, A50
Goldsmith P. F., Yıldız U. A., Langer W. D., Pineda J. L., 2015, The Astrophysical Journal, 814, 133
Gómez-Carrasco S., Félix-González D., Aguado A., Roncero O., 2022, The Journal of Chemical Physics, 157, 084301
Hily-Blant P., Bonal L., Faure A., Quirico E., 2013, Icarus, 223, 582
Knowles P. J., Hampel C., Werner H.-J., 1993, The Journal of chemical physics, 99, 5219
Knowles P. J., Hampel C., Werner H.-J., 2000, The Journal of Chemical Physics, 112, 3106
Langer W., Velusamy T., Goldsmith P., Pineda J., Chambers E., Sandell G., Risacher C., Jacobs K., 2017, Astronomy & Astrophysics, 607, A59
Le Bourlot J., 1991, Astronomy and Astrophysics, 242, 235
Le Gal R., Hily-Blant P., Faure A., Des Forêts G. P., Rist C., Maret S., 2014, Astronomy & Astrophysics, 562, A83
Lique F., Toboła R., Kłos J., Feautrier N., Spielfiedel A., Vincent L., Chałasiński G., Alexander M., 2008, Astronomy & Astrophysics, 478, 567
Lique F., Kłos J., Alexander M., Le Picard S. D., Dagdigian P., 2018, Monthly Notices of the Royal Astronomical Society, 474, 2313
Maret S., Bergin E., Lada C., 2006, Nature, 442, 425
Monteiro T. S., Flower D. R., 1987, MNRAS, 228, 101
Orlikowski T., Alexander M., 1984, Journal of Physics B: Atomic and Molecular Physics, 17, 2269
Pauly H., 1979, in , Atom-Molecule Collision Theory. Springer, pp 111–199
Persson C. M., et al., 2014, Astronomy & Astrophysics, 568, A37
Peterson K. A., Woon D. E., Dunning Jr T. H., 1994, The Journal of chemical physics, 100, 7410
Roueff E., Lique F., 2013, Chemical reviews, 113, 8906
Schöier F. L., van der Tak F. F., van Dishoeck E. F., Black J. H., 2005, Astronomy & Astrophysics, 432, 369
Shen V., Siderius D., Krekelberg W., Hatch H., retrieved <09/30/2022>, NIST Standard Reference Simulation Website
Soldán P., Hutson J. M., 2002, The Journal of chemical physics, 117, 3109
Tayal S., 2011, The Astrophysical Journal Supplement Series, 195, 12
Van der Tak F., Black J. H., Schöier F., Jansen D., van Dishoeck E. F., 2007, Astronomy & Astrophysics, 468, 627
Werner H.-J., et al., 2020, The Journal of Chemical Physics, 152, 144107
van der Tak F. F. S., Lique F., Faure A., Black J. H., van Dishoeck E. F., 2020, Atoms, 8, 15

This paper has been typeset from a TEX/LATEX file prepared by the author.

[4] https://emaa.osug.fr/,

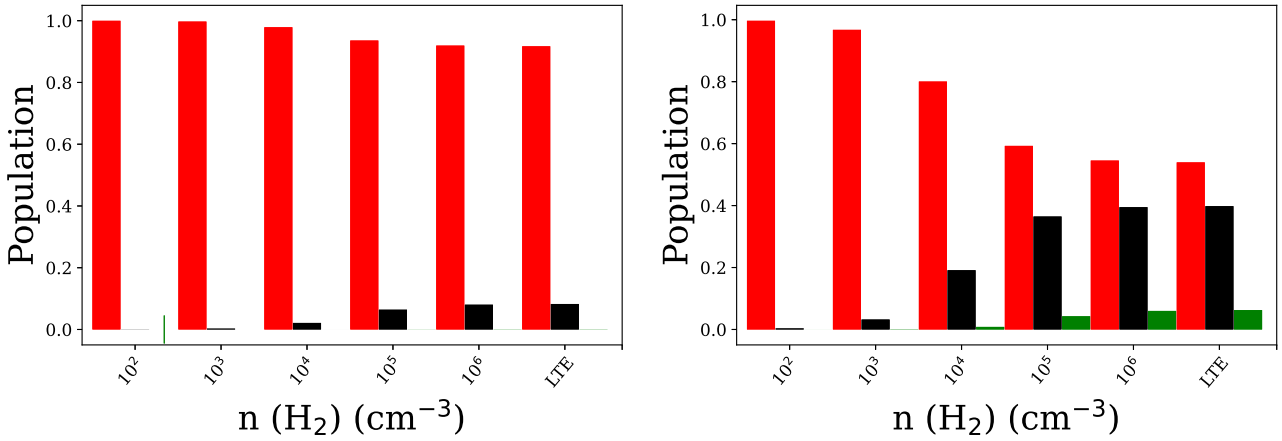

Figure 10. Population level for $^3P_0$, $^3P_1$ and $^3P_2$ states at 20K (left) et 50K (right) as a function of the density of neutral species (H_2 and He, respectively in proportions 90% and 10%). LTE conditions correspond to a density of 10^{12} cm^{-3}.